Postprint of: Mroziński A., Molin S., Karczewski J., Miruszewski T., Jasiński P.: Electrochemical properties of porous Sr0.86Ti0.65Fe0.35O3 oxygen electrodes in solid oxide cells: Impedance study of symmetrical electrodes. INTERNATIONAL JOURNAL OF HYDROGEN ENERGY. Vol. 44 (2019), iss. 3, p. 1827-1838. DOI: 10.1016/j.ijhydene.2018.11.203

Electrochemical properties of porous $Sr_{0.86}Ti_{0.65}Fe_{0.35}O_3$ oxygen electrodes in solid oxide cells: impedance study of symmetrical electrodes

A. Mroziński[1*], S. Molin[1], J. Karczewski[2], T. Miruszewski[2], P. Jasiński[1]

[1]Faculty of Electronics, Telecommunications and Informatics,
Gdansk University of Technology, Gdansk, Poland

[2]Faculty of Applied Physics and Mathematics,
Gdansk University of Technology, Gdansk, Poland

* Corresponding author: aleksander.mrozinski@pg.edu.pl

Keywords:

oxygen electrode; solid oxide cell; perovskite; electrical conductivity;

Abstract:

This work evaluates porous $Sr_{0.86}Ti_{0.65}Fe_{0.35}O_3$ (STF35) as a possible oxygen electrode material for Solid Oxide Cells. The powder synthesis was performed by solid state method. Characterization included DC electrical conductivity study of sintered bulk samples and impedance spectroscopy study of symmetrical electrodes deposited on gadolinium doped ceria substrates. Measurements were carried out in atmospheres with different pO_2 levels: 0.1% to 20% O_2. Detailed equivalent circuit analysis was carried out in order to clarify the reaction pathway on porous electrode, which extends knowledge available for dense model electrodes. At 800 °C in 21 % O_2, the DC electrical conductivity of STF35 pellet was 0.6 S cm^{-1} and the polarization resistance of the electrode in the symmetrical cell was ~100 mΩ cm^2. Detailed impedance spectroscopy studies revealed that the largest contribution (~80%) towards the polarization resistance is due to oxygen adsorption, which is limiting the oxygen reduction performance of the porous STF35 electrode. These results show the applicability of advanced impedance analysis methods (e.g. Distribution of Relaxation Times - DRT) for description of complex impedance electrode phenomena of porous electrodes.

Introduction

Solid oxide cells employ porous electrodes for reduction/oxidation of gaseous species. For the hydrogen side electrode a composite of nickel and yttria stabilized zirconia (Ni-YSZ) has been used successfully for many years [1,2], but alternative materials are also sought [3–5]. Electrochemical performance of the cells is often described to be limited by a sluggish oxygen reduction/oxidation reaction [6,7], thus research on the oxygen electrode materials is very active [8–10]. Perovskite materials are dominating the solid oxide cells oxygen electrode materials, where both high ionic and electronic (mixed ionic electronic conductors - MIECs) conductivities are required for highly performing electrodes. Among the perovskites, doped strontium titanates are very versatile materials, which can find use both for the hydrogen and oxygen electrodes in high temperature fuel cells [11–15]. Among the possible Ti substitutions, iron has been studied extensively, especially in the field of resistive oxygen gas sensors [16] and as a model MIEC perovskite. Perovskites with a general formula $SrTi_{1-x}Fe_xO_3$ (STFx) have been studied as model oxygen conductors by group of Tuller [17–20] and Ellen-Tiffee [21,22]. STF has high oxygen ion conductivity, even higher than reported for the typical oxygen electrode materials [23]. At 800 °C, oxygen ion conductivity of STF35 is ~0.035 S cm^{-1}, whereas for the state-of-the-art La0.6Sr0.4Co0.2Fe0.8O3 (LSCF) reported ionic conductivity is 0.008 S cm^{-1} [23]. Material with Fe = 0.35 exhibits an interesting property of a zero temperature coefficient of resistivity (zero-TCR). Namely, in a specific temperature range (700 °C-900 °C), electrical conductivity of the material does not depend on the temperature, only on the pO_2, which makes it a very interesting for practical applications for example in lean burn engines exhaust sensors [24,25].

STF has been also evaluated as a possible hydrogen electrode by Nenning et al. [26]. Recently, STF also found use as a mixed-conductor in oxygen permeation membranes [27–29]. Important feature of STF materials is the abundance of the forming elements (Sr, Ti, Fe), thus low price and wide availability. In comparison to other good ionic conductors containing e.g. Co, Ni, it does not contain harmful/carcinogenic elements, which is also considered an important factor [30,31].

Detailed description of the electronic structure of $SrTi_{1-x}Fe_xO_3$ has been given by Rothschild et al. [21]. At high partial pressures of oxygen it is a p-type conductor, at intermediate pO_2 an ionic conductor and at low pO_2 an electronic conductor. The levels of electronic conductivity increase with an increasing Fe/Ti ratio. The results were consistent with the reduced band gap and reduction enthalpies caused by substitution of Ti^{4+} by Fe^{3+}. For 1 at.% Fe doped $SrTiO_3$, total conductivity at 900 °C in air is below 10^{-2} S cm^{-1}, whereas for dense STF35 it is ~1 S cm^{-1} and for pure $SrFeO_3$ > 10 S cm^{-1} [32,33].

One of the possible large disadvantages of using STF35 in fuel cells is its relatively low electronic conductivity. Reported values are between 0.3 – 1 S cm^{-1} at 800 °C, much lower than for LSCF (>300 S cm^{-1}). Thus the practical applicability of STF is questionable, but its physicochemical properties and their influence on electrocatalytic performance are of basic interest [17–19,34,35]. It is still not elucidated to what extent the ionic and electronic conductivities influence the electrocatalytic properties of oxygen electrodes [35]. Yoo and Bouwmeeter evaluated oxygen surface kinetics of STF and concluded, that the ionic conductivity controls the rate of oxygen exchange [36]. Argirusis et al. have evaluated oxygen surface exchange and diffusion of STF, they found that at temperatures below 800 °C the slow oxygen surface exchange was hindering the electrochemical performance [22]. The same conclusion was made by Jung and Tuller [18,19]. Surface exchange limitation is typical for most mixed-ionic electronic conductors, but the underlying processes are yet to be described in details. Most of the basic studies dealt with model dense electrodes, where the contact area was carefully tailored. No studies have analyzed the STF as a possible porous electrode in details, describing what are the effects of the surface exchange limitation on their performance.

STF35 has been studied as a possible cathode material for Solid Oxide Fuel Cells (SOFCs) by our group before [37]. In this case a reasonably good performance of 120 mΩ cm^2 has been achieved on yttria stabilized zirconia (YSZ) electrolyte at 800 °C. The result was reached despite a chemical reaction of STF with YSZ. Formation of a $SrZrO_3$ phase between Sr and Zr containing materials is a well known phenomena [38,39], that leads to reduction in electrochemical performance of the electrodes. This can be mitigated by using doped ceria based electrolytes or application of ceria barrier layers on YSZ electrolytes [40]. Therefore it has been decided to study the electrochemical properties of STF35 on ceria based electrolyte in this work.

Oxygen reduction reaction (ORR) on solid state electrodes is an often studied reaction [41]. Though several decades of research have passed, still no clear and concise general description is available. Due to the large number of possible intermediate species several mechanisms and models have been postulated. Analysis of model compounds like STF35 can deliver new insight into the mechanisms, thus this material has been extensively studied, especially in the form of dense, thin electrodes with well-defined geometrical dimensions [42,43]. A typical general oxygen reduction pathway starts with gaseous oxygen (O_2) that has to be adsorbed on the surface, dissociate into oxygen atoms and then it has to be incorporated into the crystal lattice through the surface. The details of the adsorbate (charge level) and incorporation mechanisms are still subjected to discussions [20,44].

In this work electrochemical properties of porous STF35 electrodes are studied based on CGO electrolyte substrates. Our group has previously studied STF35 electrode on YSZ electrolyte, where chemical reaction between Sr and Zr occured. It is therefore interesting to evaluate the properties of STF35 on CGO, where no reactions take place. In this work, the effect of the sintering temperature on the polarization resistance of symmetrical STF/CGO/STF electrodes is studied. Factors limiting electrochemical performance are evaluated by performing impedance spectroscopy measurements in atmospheres with different oxygen content and at different temperatures. Advanced impedance analyses methods are employed in order to propose physically relevant electrical equivalent circuit. Results obtained in this work are an extension of results obtained on model thin dense electrodes and further clarify the current understanding of the limiting processes.

Materials and methods

Material synthesis

$Sr_{0.86}Ti_{0.65}Fe_{0.35}O_{3-\delta}$ (STF35) powder was prepared by a conventional high temperature solid state reaction method. Strontium carbonate ($SrCO_3$), iron (III) oxide (Fe_2O_3) and titanium dioxide (TiO_2) were used as the starting reagents (purity >99%, all from Sigma-Aldrich, USA). The weighed powders were mixed in a planetary ball mill (Fritsch Pulverisette 7, using 80 ml zirconia container with 5 mm alumina balls) in ethanol for 12 h with rotational speed of 200 rpm. Dried, mixed powders were uniaxially pressed (90 MPa) into pellets, which were sintered at 1200 °C for 15 h (with cooling/heating rate 3 $°\cdot min^{-1}$). Next, the pellets were re-ground and again pressed for the second sintering step at the same temperature conditions. Finally, the fabricated powder was re-ground and ball milled in two stages using 3 mm YSZ balls. The first milling was conducted with rotational speed of 400 rpm and the second milling with rotational speed of 600 rpm each for 8 h. Such obtained powder was used throughout the study to prepare the samples for further characterization.

Samples preparation

For the electrical conductivity measurements, STF35 powder was uniaxially pressed into 16 mm diameter pellets under a pressure of 70 MPa. The pellets were sintered at 1200 °C for 2 h (with cooling/heating rate 3 $°\cdot min^{-1}$). The obtained pellets had a diameter of 12 mm with 94 % of theoretical density (measured by Archimedes method).

Symmetrical electrodes for impedance analysis were prepared on gadolinium doped ceria (CGO) substrates. CGO pellets were made from a commercial powder (GDC-20K, DKKK Japan), which was compacted under a pressure of 70 MPa and sintered at 1400 °C for 8 h. After the sintering, CGO substrates had diameters of 13 mm and 98 % of the theoretical density. The obtained pellets were grinded to approximately 0.6 mm thickness and polished to obtain a smooth surface and remove any contaminants.

STF35 paste for painting of the symmetrical electrodes was made from the fabricated STF35 powder mixed with a paste vehicle system ESL403 (Electro-Science Laboratories, USA). Paste consisted of 65 wt.% of powder and 35 wt.% of the vehicle mixed in a mortar. Circular STF35 electrodes were brush-painted on both sides of the polished CGO pellets. The thickness of the electrodes was 30 μm with a diameter of 7 mm. Painted electrodes were slowly dried at room temperature and at 60 °C and at 130 °C. Finally, electrodes were sintered for 2 hours at 900/950/1000/1050 °C in air with an intermediate dwell step at 600 °C for 1 hour to remove the binder (with heating rate 1.5 $°\cdot min^{-1}$ to 600 °C and in the following steps heating/cooling rates 2 $°\cdot min^{-1}$). Surface of the sintered electrodes were coated with platinum current collector (about 5 μm thick) by brush painting Pt paste (ESL 5542, Electro-Science Laboratories, USA). Platinum electrodes were fired at 900 °C for 10 min with heating/cooling rate 3 $°\cdot min^{-1}$.

Compositional and microstructural analysis

The phase composition of the investigated STF35 powder was analyzed by X-ray diffractometry (XRD) at room temperature. XRD spectra of the powder was collected using Philips X'Pert Pro MPD diffractometer with Cu K_α (1.542 Å) radiation in a standard 2θ Bragg-Brentano geometry. The diffraction patterns were analysed with the Rietveld refinement method using the HighScore Plus software package [45]. The Pseudo – Voigt peak shape function was used during the refinement. Crystallographic structure of STF35 has been drawn using Vesta software package [46].

Cross sectional images of the symmetric cells samples were obtained using a FEI Quanta FEG 250 Scanning Electron Microscope (SEM) with an accelerating voltage of 10 kV in a high vacuum mode. SEM was operated with a backscattered electron (BSE) detector. Chemical composition of samples was determined using the energy-dispersive X-ray (EDX) spectroscopy using the EDAX Genesis APEX 2i with Apollo X SDD spectrometer at 20 kV.

For SEM imaging of the cross sections of symmetrical cells were embedded in the epoxy resin (EpoFix, Struers, Denmark). The epoxy was polished down to 1 μm diamond suspension finish (Struers, Denmark) and rinsed with isopropanol. The surface of polished epoxy was coated with carbon before imaging.

Electrical and electrochemical performance analysis

DC electrical conductivity measurements were performed on STF35 pellets (~12 mm diameter, ~1 mm thick) by the Van der Pauw method. Prior to measurements, surfaces of the STF35 pellets were slightly polished and silver point contacts (DuPont 4922 N, USA) were painted at the edges. The resistance measurements were performed using Keithley 2400 SourceMeter with custom software (working in the potentiostatic mode at 50 mV). Measurement temperature range was between 900 °C and 200 °C. Studies were performed at different oxygen partial pressures (20 %, 1 % and 0.1 %) under humidified (~4 vol.%) gas flow rate of 50 $ml \cdot min^{-1}$.

Area Specific Resistance (ASR) of the prepared symmetrical cells was measured by electrochemical impedance spectroscopy (EIS) using Novocontrol Alpha-A with an excitation amplitude of 25 mV in the frequency range of 1 MHz to 50 mHz. Firstly, the evaluation of the effects of the sintering temperature on the resulting ASR was carried out. The measurement temperature range was between 800 °C and 500 °C in stationary air. This temperature range is a typical operating temperature of intermediate-temperature SOFCs. Based on the EIS results, a more detailed analysis of the impedance of symmetrical cells with oxygen electrode sintered at 1000 °C were carried out. Measurements were performed in different oxygen partial pressures (20 %, 10 %, 5 %, 1 %, 0.1 % and 0.01%) in the temperature range 800 °C - 600 °C. For this purpose Solartron 1287/1260 system was used. Applied measurement conditions were the same as in the previous measurement using Novocontrol. EIS data analysis was performed using Elchemea Analytical (www.elchemea.dk, Technical University of Denmark) software [47]. Distribution of Relaxation Times analysis has been performed by using DRTools Matlab GUI [48–50].

Results and discussion

Analysis of $Sr_{0.86}Ti_{0.65}Fe_{0.35}O_{3-\delta}$ powder

The fabricated STF35 powder was analyzed by XRD in order to confirm the formation of the cubic perovskite oxide phase. The XRD pattern of the STF35 powder, measured at room temperature, is shown in Figure 1 A.

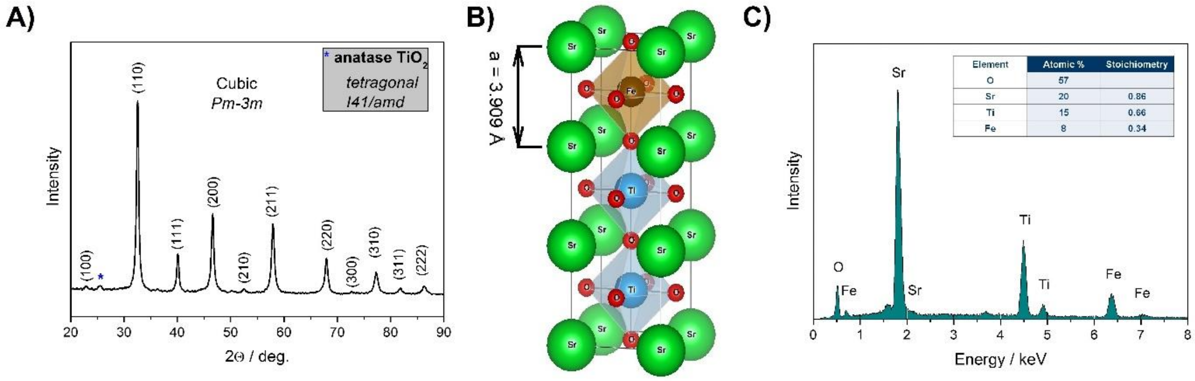

Element	Atomic %	Stoichiometry
O	57	
Sr	20	0.86
Ti	15	0.66
Fe	8	0.34

Figure 1. X-ray diffractometry of the fabricated powder (A), crystallographic structure of STF35 (B) and energy dispersive x-ray spectra of the sintered pellet used for electrical conductivity study (C).

All the diffraction peaks, except a small one at 2θ = 25.6 ° (*), can be identified as strontium titanate, with a cubic crystal structure ($Pm\bar{3}m$) (Inorganic Crystal Structure Database #186710). The small detected peak (at 2θ = 25.6 °) is related to titanium dioxide TiO_2 in the anatase form (tetragonal, *I41/amd* space group), called also as Magnéli phase. The presence of this phase in the structure is strongly related to the nonstoichiometry of strontium (Sr/Ti<1 in $SrTiO_3$), what was previously reported in the literature [51–53]. This result indicates the presence of strontium vacancies V_{Sr}'' in the sample. XRD pattern was subjected to a Rietveld refinement based on the $Pm\bar{3}m$ cubic space group. Calculated average lattice constant is a = 3.90882(1) Å, with Goodness of Fit parameter (GoF) = 1.37. Crystal structure of STF35 perovskite is shown in Figure 1 B. Mixed valence Fe cations partially substitute Ti^{4+} ions in the center of oxygen octahedra. For comparison lattice constant of pure $SrFeO_3$ and $SrTiO_3$ is occur a = 3.851 Å and a = 3.905 Å respectively [54,55]. Thus, addition of Fe into $SrTiO_3$ structure caused the lattice should decrease its size. In this work, the obtained lattice parameter slightly deviates from the reported ones and seems to be higher. The observed higher value of average lattice constant than reported for a pure and undoped $SrTiO_3$ is probably caused by appearance of strontium vacancies V_{Sr}'' in the structure.

Chemical composition of the bulk STF35 pellet is presented in Figure 1 C. EDX analysis shows the elements present (Sr, Fe, Ti and O). The averaged atomic percentage of the sintered STF35 pellet is 20 % Sr, 15 % Ti, 8 % Fe and 57 % O. Ratio of atoms in the B sublattice (Fe and Ti) is in good agreement with the calculation for STF35. Detected deficiency of Sr atoms in the A sublattice is 0.86. It does not seem to have an effect on the structure, as the perovskite cubic phase is preserved.

The effects of nonstoichiometry on the A-site in the STF35 structure were studied by group of Kharton [56–58]. By using Sr deficient materials, their physicochemical properties seem to be improved: tolerance to CO_2, increased oxygen nonstoichiometry and ionic conductivity with no loss of electronic conductivity. Kharton et. al [57] have shown that the total conductivity of $SrTi_{0.2}Fe_{0.8}O_{3-\delta}$ (STF80) practically does not depend on the presence of a Sr vacancy in the A site between 800 °C and 600 °C. The detected non-stoichiometry of the compound can potentially be responsible for the unit cell size different than reported previously for the stoichiometric compounds, as also noticed by Kharton et al. [57].

The non-stoichiometry on the A-site is an interesting feature in the case of its influence on the oxygen reduction reaction, thus the causes and possible effects of Sr deficiency will be studied separately in our future works.

Electrical conductivity measurements

Electrical conductivity measurement results of sintered pellets are presented in Figure 2 as a function of temperature (from 900 °C to 200 °C) and in different of pO_2. The conductivity of STF35 decreases with decreasing the oxygen partial pressure, similarly with previous reports [59,60] and the expected p-type conductivity. The highest conductivity ($0.59\ S\cdot cm^{-1}$) was obtained at 900 °C in 20 % O_2 and is comparable with literature ($\sim 1\ S\ cm^{-1}$) [33]. As expected, the conductivity is only slightly dependent on temperature between 900 °C and 700 °C. The calculated activation energy (E_a) for this temperature range is $8\ kJ\cdot mol^{-1}$. Below 700 °C, the total conductivity decreases with decreasing temperature and activation energy increases considerably ($E_a = 38.5\ kJ\cdot mol^{-1}$) which probably is connected with localization of atomic levels and bandwidth changes [56]. Steinsvik et al. [61] and Rothschild et al. [21] have extensively studied electrical and defect properties of $SrTi_{1-x}Fe_xO_{3-d}$. The electrical conductivity behavior is a complex interplay between the acceptor role of the iron substitution causing a decrease of the band gap and decreased activation energy for oxygen vacancy migration. Interestingly, the electronic transport seems to have a band-like behavior, with decreasing mobilities at high temperatures, rather than the small polaron transport model.

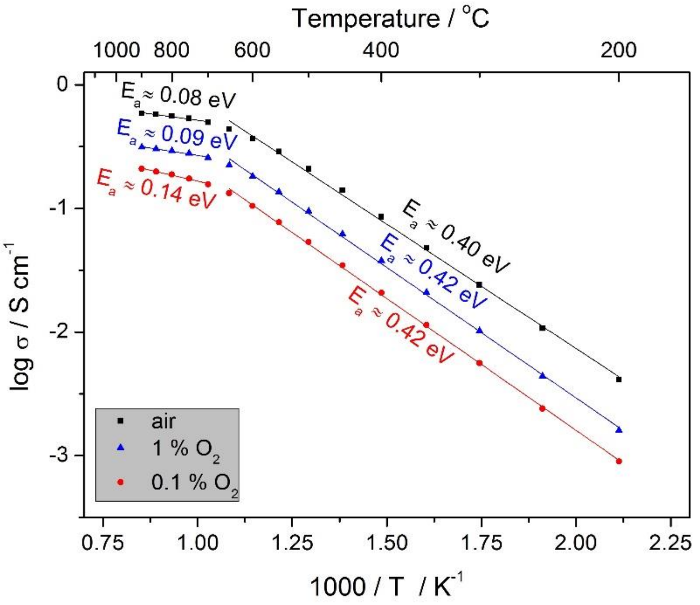

Figure 2. Electrical conductivity plots of sintered STF35 pellet in 21 %, 1% and 0.1% O_2.

Electrochemical characterization of symmetrical cells

Effects of the electrode sintering temperature on the electrochemical performance were evaluated by impedance spectroscopy of symmetrical electrode samples. Measurements were carried out in air in the temperature range 800 °C-500 °C which is typical for operating temperature of intermediate-temperature SOFCs. Spectra measured at 800 °C are presented in Figure 3. The lowest sintering temperature (900 °C) resulted in the highest ohmic resistance. Increasing sintering temperature leads to lowering of the ohmic resistance. Interestingly, the polarization resistance seems unaffected by the sintering temperature ($R_{pol} \sim 100\ m\Omega\ cm^2$). For the sintering temperature of 1050 °C severe cracking of the electrode occurred, caused by electrode shrinkage due to sintering. ASR value is comparable with literature reports for STF with higher amount of Fe (0.85) which seems appealing [62].

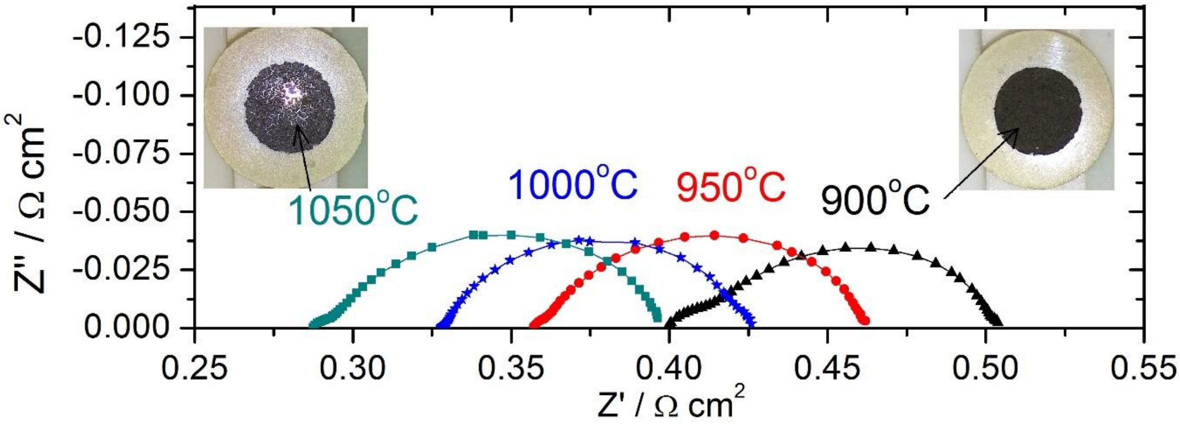

Figure 3. Impedance spectra of symmetrical STF35 electrodes sintered at different temperatures measured at 800 °C in air.

Temperature dependence of the ohmic contribution of differently sintered samples is shown in Figure 4 A. Electrodes with different sintering temperature show different conductivity values (for fixed temperature), as was the case at 800 °C, but have similar activation energy ~65 kJ mol^{-1}. For the sintering temperature of 1000 °C, at 800 °C a resistance of 0.65 Ω cm^2 was obtained and at 500 °C a resistance of 10 Ω cm^2 was measured. Activation energy and the level of resistance are in line with the values reported for doped ceria compounds [63]. Ohmic contribution can be thus ascribed to the series connection of the resistance of the ceria pellet and the resistance of the porous electrode, through which the current is flowing.

Polarization resistance of the STF35 electrode plotted as a function of temperature is shown in Figure 4 B. Polarization resistance is very similar for all sintering temperatures at all studied temperatures. The activation energy of the polarization resistance is ~136 kJ mol^{-1}. It is much higher than the activation polarization of the electrical conductivity of the bulk material. The obtained value is typical for oxygen electrodes [37,64,65].

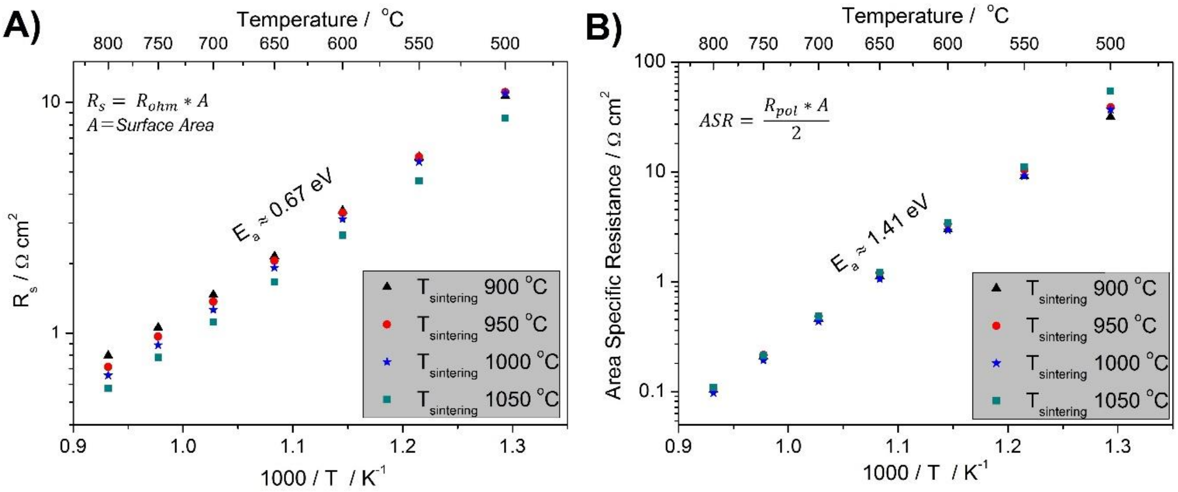

Figure 4. Series (A) and polarization (B) resistance of the symmetrical STF35 electrodes sintered at different temperatures as a function of temperature in air

Post-mortem SEM

Post-mortem SEM images of cross section of symmetric cells with STF35 electrodes measured by EIS method are presented in Figure 5 A-C. Representative images of electrodes sintered at 950 °C, 1000 °C and 1050 °C are included for comparison. There is no visible difference in the microstructures of the porous-part of the STF35 electrode sintered at different temperatures. However the CGO-STF35 interface appears to be considerably influenced by the sintering temperature. A dense interface layer with thickness ~500 nm is formed for electrodes sintered >1000 °C. This layer improves the electrical contact as the ohmic resistance was decreased for these samples (visible in Figure 3). EDX analysis of the chemical composition (not shown here) of the interface layer did not show any segregation of elements, its chemical composition is similar to the chemical composition of the porous electrode. As we have previously reported, there is no negative reaction (phase forming) between STF35 and CGO [66], thus the interface layer is not expected to negatively influence the electrochemical performance of the porous electrode. As shown in Figure 3, shrinkage caused by sintering of the electrode above 1000°C leads to its visible cracking, prohibiting from practical use in real cells. Good electrochemical response of the cracked electrode might be partially due to platinum current collector coverage, filling the cracks and the dense interfacial layer, facilitating oxygen reduction/oxidation reaction at the interface.

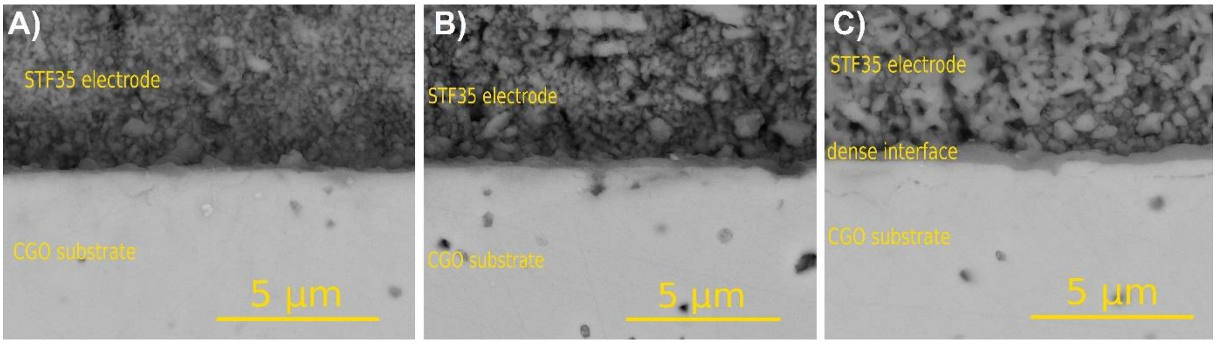

Figure 5. SEM images of cross sections of porous STF35 electrodes sintered at 950 °C (A), 1000 °C (B) and 1050 °C (C)

Oxygen reduction mechanism

In order to describe electrode properties in more details, a thorough electrochemical evaluation of the electrode sintered at 1000 °C was performed. In order to describe the possible governing physico-chemical processes, measurements were carried out in atmospheres with different oxygen content (20%, 10%, 5%, 1%, 0.1%, 0.01%) in the temperature range 800 °C-600 °C.

Studying electrode resistances as a function of the gas oxygen content can be a powerful tool for determining possible electrode mechanisms. As has been described in the literature [67,68], chemical and electrochemical processes can be distinguished based on their dependency on the pO_2. By plotting polarization resistance contributions as a function of pO_2 in a log-log plot, the slope "n" will be representative for the possible mechanism ($1/R \sim (pO_2)^n$). For n=1, gas diffusion of molecular oxygen process is expected, n=0.5 implies the contribution of atomic oxygen. For n=0.25 a charge transfer/adsorption process is the likely contribution. Thus by careful examination of the impedance data, differentiation between the occurring processes can be made.

For description of the obtained results, first a physically sound equivalent circuit had to be determined. By examination of the spectra it was assumed that it consisted of at least 3 resistive-capacitive elements. For validation of the assumption, a distribution of relaxation times method was used. All measured spectra were analyzed with DRTools script. In Figure 6 selected, representative DRT spectra are shown. Figure 6 A shows oxygen content dependence of DRT spectra at 800 °C. At lowering of pO_2 a new contribution at low frequency clearly occurs. At mid-frequency pO_2 dependent element is also visible. At high frequencies a relatively smaller contribution can be found. It seems to have a non-symmetrical shape, typically ascribed to Gerischer type elements [69]. Figure 6 B presents temperature dependence of DRT spectra obtained at 0.1% oxygen content, so that the low frequency contribution is visible. Low- and mid-frequency contributions are clearly present, with a possible Gerischer type element at high frequency (visible at 700 °C). Based on careful DRT analysis at different conditions, an equivalent circuit consisting of R_s-G-($R_{mid}CPE_{mid}$)-($R_{low}CPE_{low}$) was proposed (R_s – series resistance, G – Gerischer element, CPE – Constant Phase Element). At 700 °C in 0.1% O_2 the characteristic frequencies (contributions peak – frequency at highest Z” values) of the contributions are ~17 Hz, ~1 Hz and ~0.2 Hz, as also visible in DRT plots. The obtained fitting had very high quality. Representative impedance spectra (measured at 700 °C and 800°C at 0.1% oxygen) are shown in Figure 7 together with the results of the fitting. It should be noted, that also other possible equivalent circuits were initially analyzed and evaluated, e.g. a triple (RCPE) connection, it resulted in visibly worse fitting and higher chi-squared values. For the proposed equivalent circuit chi-squared parameter was mostly $<10^{-5}$, representing a good fit. For some measurement conditions, the contributions became negligibly small, so the parameters were either locked or removed from the analysis. The same equivalent circuit as presented here has been also used by the group of Boukamp [70,71] for analysis of LSCF electrodes. The series resistance typically can be ascribed to the ohmic resistance of the electrolyte substrate, Gerischer element to some surface/solid state diffusion limited phenomena and the two R-CPE elements to possible other phenomena, including for example adsorption, gas diffusion and others, to be determined from detailed impedance measurements.

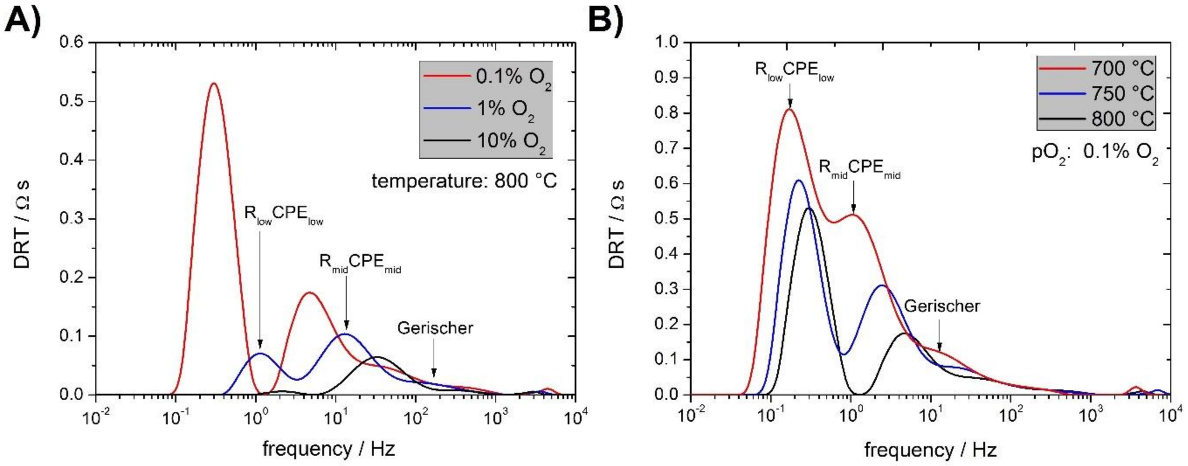

Figure 6. Exemplary distribution of relaxation times plots of impedance of a symmetrical STF35 electrodes as a function of the oxygen partial pressure at 800 °C (A) and as a function of temperature at 0.1% O_2 (B).

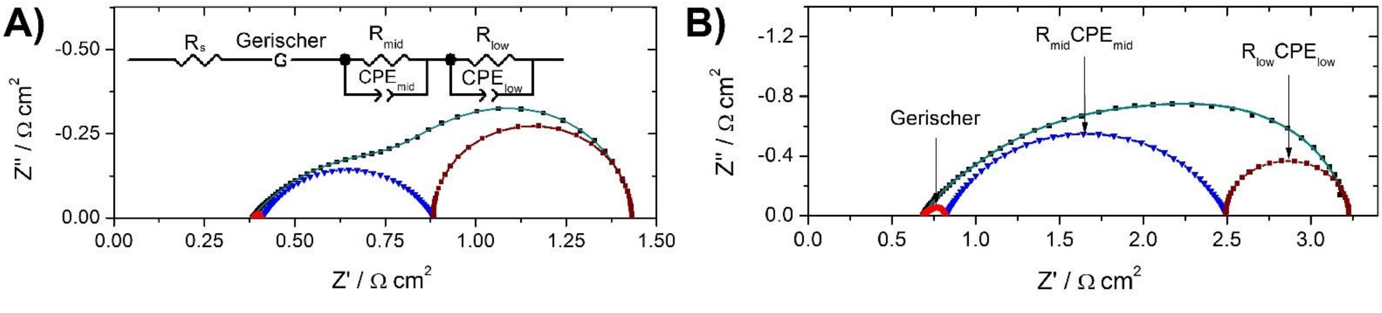

Figure 7. Exemplary impedance spectra of a symmetrical STF35 electrode measured at 800 °C (A) and 700°C (B) in 0.1% O_2 shown with an equivalent circuit and individual contributions of the respective fitting elements.

Based on the measured spectra (as a function of temperature and pO_2) and the selected equivalent circuit, all data was fitted and the results are presented in the following figures. Moreover, all values of the equivalent circuit elements for measurement at 700 °C at different oxygen partial pressures are given in Table 1.

Figure 8 presents the dependence of the series resistance on the oxygen partial pressure. Temperature dependence was presented in Figure 4A. Only slight dependence of the resistance on pO_2 is visible, as expected for the ohmic contribution. Electrical conductivity of STF35 depends on the pO_2, thus atmosphere changes will also influence the ohmic contribution of the porous electrodes. Lowering the pO_2 results in increased resistance, in line with the electrical conductivity results presented in Figure 2.

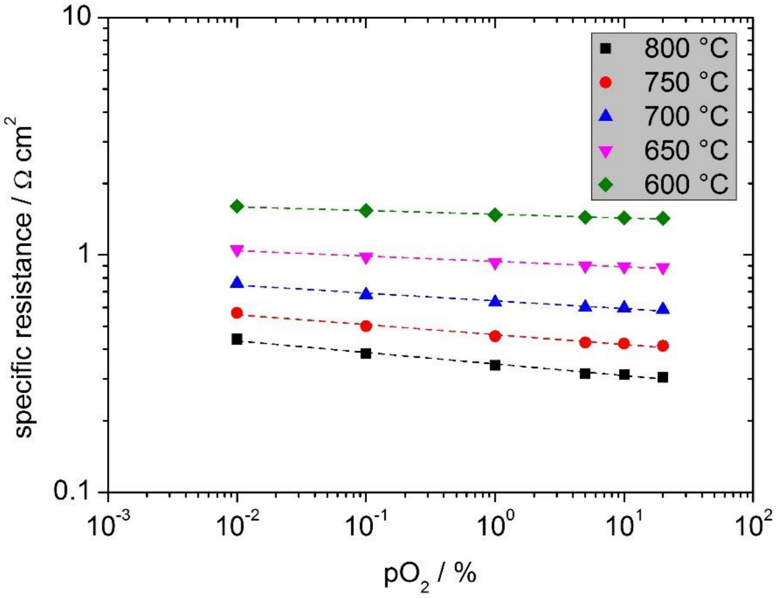

Figure 8. pO_2 and temperature dependence of series resistance of symmetrical STF35 electrodes on CGO substrate.

Dependencies of the Gerischer element on temperature and oxygen content are presented in Figure 9 A-D. The rate constant parameter "k" is strongly dependent on the temperature with activation energy ~1.55 eV, whereas the admittance parameter "Y" shows only a slight dependence on the temperature (activation energies around ~0.07 eV). In the case of oxygen partial pressure dependence, rate constant parameter increases with an increase of the oxygen content with a ~1/6 slope, whereas the admittance parameter seems not dependent on the oxygen partial pressure. The magnitude of the Gerischer element resistance is roughly ~15 mΩ cm² at 800 °C, and it is independent of the oxygen partial pressure. Gerischer type elements are often used in modelling of porous SOFC electrodes – the popular Adler model is based on this element [72,73], often used for modelling of LSCF electrodes. In case of the limiting electrode processes being the chemical surface exchange and/or solid state oxygen diffusion in the bulk, it will be represented as a Gerischer element in the impedance spectra. Hildenbrand and Boukamp used a similar equivalent circuit for description of porous LSCF electrodes [70,71].

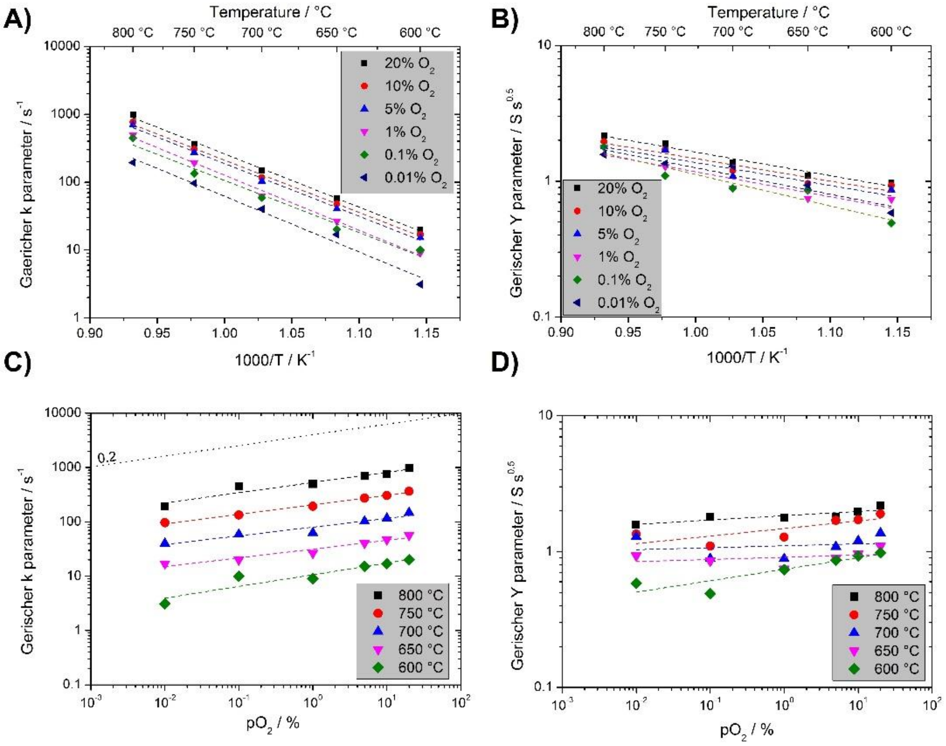

Figure 9. Plots of the calculated rate constant k and admittance Y parameters of the high frequency Gerischer element as a function of temperature (A and B respectively for k and Y parameters) and pO2 (C and D respectively for k and Y parameters).

Following the Gerischer element are the two R-CPE elements. The dependencies of their resistance on temperature and oxygen gas content are presented in Figure 10. Medium frequency resistance is a thermally activated process with E_A~1.45 eV with oxygen dependence of ~0.3. According to theoretical considerations, such pO_2 dependence happens possibly due to adsorption of oxygen and surface exchange (dependence of 0.25). In the case of dissociative adsorption (involvement of atomic oxygen), the expected oxygen dependence is ~0.5. Therefore it seems that the non-dissociative adsorption of oxygen contributes the most to the polarization resistance of the STF35 electrode. At 800 °C in 20 % oxygen the resistance of the medium frequency contribution is ~80 mΩ cm^2, which is ~80% of the total polarization resistance at this temperature. Adsorption might be limited by different factors, e.g. slow removal of adsorbed oxygen atoms from the surface caused by slow incorporation into the lattice. Activation energy of the Gerischer rate constant parameter is close to the measured activation energy of the medium frequency contribution, so both elements seem connected together, the rate limiting adsorption determines the bulk diffusion. Equivalent capacitance of this contribution is presented in Figure 11. With increasing pO_2, capacitance decreases, measured values are between 50-100 mF cm^{-2}. Similar capacitances of the medium frequency contributions have been measured by Hildenbrand et al. [71] and Dailly et al. [74]. Values in the range of ~mF cm^{-2} appear typical for adsorption processes [42,75]. Argirusis et al. have measured oxygen incorporation and diffusion in STF35 ceramics [22]. They described that at temperatures <750°C oxygen surface transfer becomes slow. The activation energy of the oxygen surface exchange coefficient k* was determined to be ~1.66 eV, whereas the activation energy of the diffusion coefficient D* was ~0.92 eV. The activation energy of the medium frequency contribution found in this work is thus quite similar to the surface exchange activation energy.

The low frequency R-CPE contribution does not show temperature dependence and shows strong oxygen partial pressure dependence, $1/R \sim pO_2$. These characteristics and measured values are typical for gas diffusion resistance in porous electrodes. This is further evidenced by very high chemical capacitance, as shown in Figure 11, from 0.4 F cm^{-2} to ~8 F cm^{-2}, similarly to values reported by

Hildenbrand [71] and Santos-Gomez et al. [76]. Gas diffusion contribution constitute only a very small contribution to total polarization resistance, R~10 mΩ cm^2 at 800 °C in 20% O_2. If required, gas diffusion resistance can be further minimized by modification of electrode microstructure.

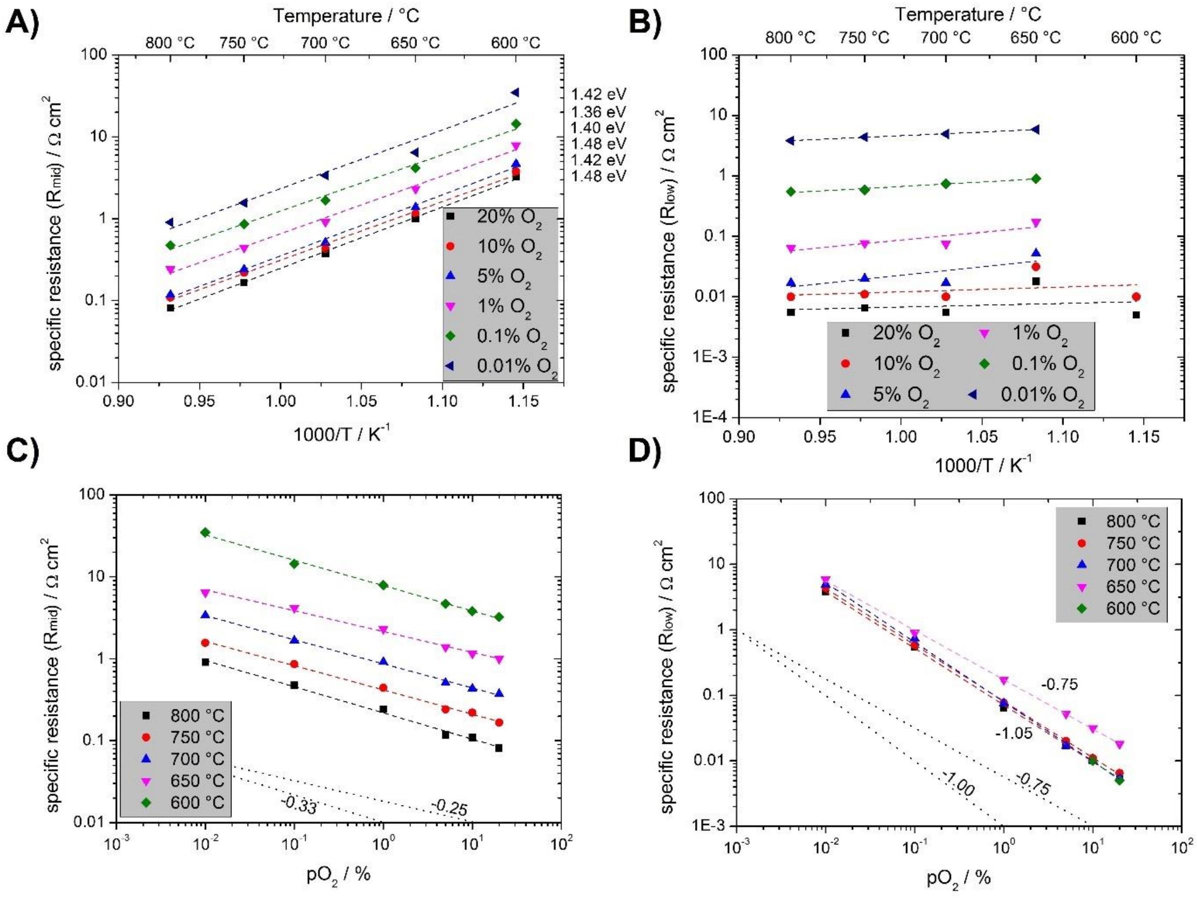

Figure 10. Plots of the calculated resistances of the medium and low frequency contributions as a function of temperature (A and B respectively for R_{mid} and R_{low}) and pO2 (C and D respectively for R_{mid} and R_{low}).

Table 1 – calculated parameters for 700 °C in different oxygen partial pressures

	R_s (Ω cm^2)	Gerischer k parameter (s^{-1})	Gerischer Y parameter (S $s^{0.5}$)	R_{mid} (Ω cm^2)	Equivalent C_{mid} (F cm^{-2})	R_{low} (Ω cm^2)	Equivalent C_{low} (F cm^{-2})
20 % O_2	0.59	147.7	1.37	0.37	0.055	0.0055	6.86
10 % O_2	0.60	116.7	1.20	0.43	0.061	0.0100	5.26
5 % O_2	0.60	103.1	1.09	0.51	0.066	0.0170	3.92
1 % O_2	0.63	62.9	0.89	0.92	0.088	0.0750	2.71
0.1 % O_2	0.69	59.2	0.89	1.67	0.106	0.7381	1.33
0.01 % O_2	0.76	40.2	1.28	3.39	0.165	4.9330	1.00

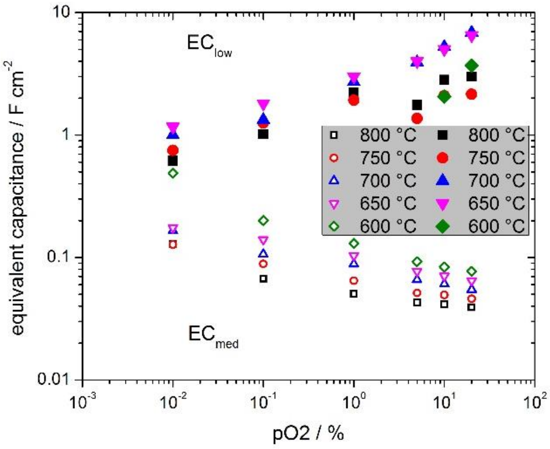

Figure 11. Plots of the calculated equivalent capacitances of the medium (open symbols) and low (closed symbols) frequency contributions at different temperatures as a function of the pO_2.

The equivalent circuit presented in Figure 7 appears to represent all data very well. Physicochemical description of all components seems well justified and comparable with the available literature data. Hypothetically, if the adsorption would be very fast, with only a negligible contribution, and not including gas diffusion resistance, the polarization resistance of the porous STF35 electrode would be only ~15 mΩ cm^2 at 800 °C in 20% O_2, which can be considered very low, similar to polarization resistance of LSCF.

Figure 12 presents the possible oxygen reduction pathways and rate limiting reactions, as has been determined in this study. Performance of porous STF35 electrodes is limited by adsorption of oxygen species, possibly hindered by slow incorporation of oxygen into the lattice. Rate determining reactions are marked with a green circle. Same limiting mechanisms have been determined for STF35 model dense electrodes [18,22,33]. Future studies will therefore be directed towards use of surface catalysts and studies of their effect on adsorption and surface exchange of the STF35, which has already shown some remarkable possibilities [22]. STF35 electrode, with its clearly defined adsorption limitation seems a very good material to determine possible role of surface modifications/catalysts.

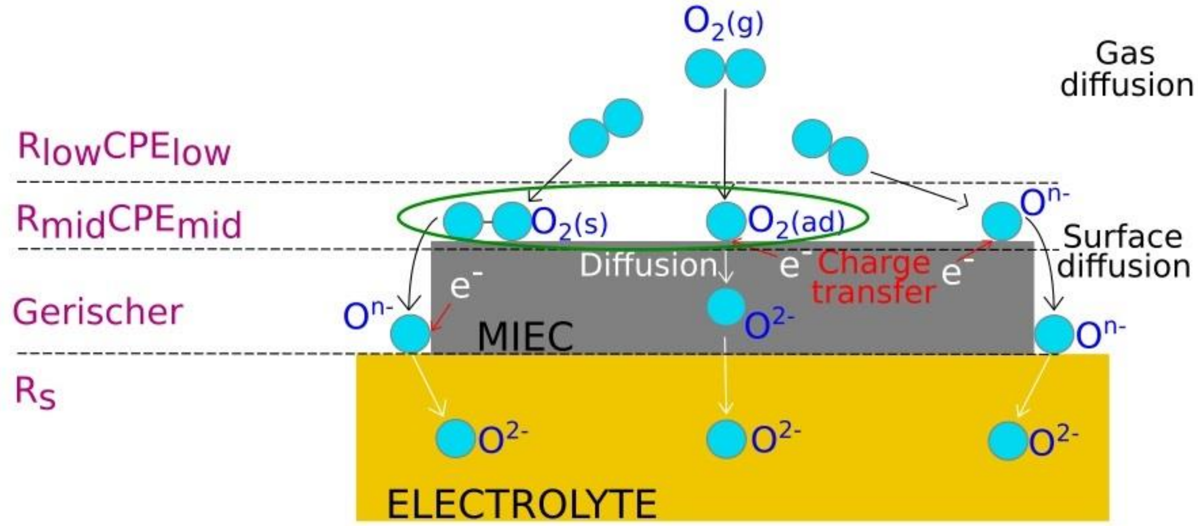

Figure 12. Schematic pathways for oxygen reduction reaction.

Conclusions

STF35 mixed ionic-electronic conductor perovskite has been fabricated and evaluated for its high temperature electrochemical properties as possible oxygen electrode in solid oxide cells. Studies were performed on symmetrical porous STF35 electrodes, whereas the studies performed so far were focused mainly on dense model electrodes. Detailed impedance spectroscopy study, performed at different temperatures and at different oxygen partial pressures revealed that the performance of the electrode is limited by oxygen adsorption, as has been previously reported for dense STF35 films. Results show that with the use of advanced analysis and appropriate measurement conditions, it is possible to use porous electrodes to study basic physico-chemical properties of materials, typically performed on dense materials fabricated by more advanced processes. It has been shown, that bulk properties of the STF materials are comparable to the state of the art LSCF cathodes. Other processes that were recognized by impedance analysis include a Gerisher type element, possibly connected to gas adsorption and solid state diffusion and gas diffusion resistance. STF35 is a very interesting model material to measure the oxygen reduction processes and its limiting factors.

Acknowledgements

This work was partly supported by project funded by National Science Centre Poland based on decision 2017/25/B/ST8/02275. This work is partly supported by a statutory grant for research from the Gdansk University of Technology.

References:

[1] da Silva FS, de Souza TM. Novel materials for solid oxide fuel cell technologies: A literature review. Int J Hydrogen Energy 2017;42:26020–36. doi:10.1016/j.ijhydene.2017.08.105.

[2] Goodenough JB, Huang Y-H. Alternative anode materials for solid oxide fuel cells. J Power Sources 2007;173:1–10. doi:10.1016/j.jpowsour.2007.08.011.

[3] Tian Y, Li J, Liu Y, Yang J, Liu B, Jia L, et al. Preparation and properties of PrBa0.5Sr0.5Co1.5Fe0.5O5+Δas novel oxygen electrode for reversible solid oxide electrochemical cell. Int J Hydrogen Energy 2018;43:12603–9. doi:10.1016/j.ijhydene.2018.03.187.

[4] Sarno C, Luisetto I, Zurlo F, Licoccia S, Di Bartolomeo E. Lanthanum chromite based composite anodes for dry reforming of methane. Int J Hydrogen Energy 2018;43:14742–50. doi:10.1016/j.ijhydene.2018.06.021.

[5] Bochentyn B, Karczewski J, Molin S, Klimczuk T, Gazda M, Jasinski P, et al. The comparison of SrTi 0.98Nb 0.02O 3-δ-CeO 2 and SrTi 0.98Nb 0.02O 3-δ-YSZ composites for use in SOFC anodes. J Electroceramics 2012;28. doi:10.1007/s10832-012-9693-8.

[6] Barfod R, Mogensen M, Klemensø T, Hagen A, Liu Y-L, Vang Hendriksen P. Detailed Characterization of Anode-Supported SOFCs by Impedance Spectroscopy. J Electrochem Soc 2007;154:B371. doi:10.1149/1.2433311.

[7] Hagen A, Liu YL, Barfod R, Hendriksen P V. Assessment of the Cathode Contribution to the Degradation of Anode-Supported Solid Oxide Fuel Cells. J Electrochem Soc 2008;155:B1047. doi:10.1149/1.2960938.

[8] Niemczyk A, Olszewska A, Du Z, Zhang Z, Świerczek K, Zhao H. Assessment of layered La2-x(Sr,Ba)xCuO4-δoxides as potential cathode materials for SOFCs. Int J Hydrogen Energy 2018;3. doi:10.1016/j.ijhydene.2018.06.119.

[9] Molenda J, Kupecki J, Baron R, Blesznowski M, Brus G, Brylewski T, et al. Status report on high temperature fuel cells in Poland – Recent advances and achievements. Int J Hydrogen Energy 2017;42:4366–403. doi:10.1016/j.ijhydene.2016.12.087.

[10] Zhang Y, Knibbe R, Sunarso J, Zhong Y, Zhou W, Shao Z, et al. Recent Progress on Advanced Materials for Solid-Oxide Fuel Cells Operating Below 500 °C. Adv Mater 2017;1700132:1700132. doi:10.1002/adma.201700132.

[11] Sunarso J, Hashim SS, Zhu N, Zhou W. Perovskite oxides applications in high temperature oxygen separation, solid oxide fuel cell and membrane reactor: A review. Prog Energy Combust Sci 2017;61:57–77. doi:10.1016/j.pecs.2017.03.003.

[12] Gazda M, Jasinski P, Kusz B, Bochentyn B, Gdula-Kasica K, Lendze T, et al. Perovskites in solid oxide fuel cells. vol. 183. 2012. doi:10.4028/www.scientific.net/SSP.183.65.

[13] Weber A, Ivers-Tiffée E. Materials and concepts for solid oxide fuel cells (SOFCs) in stationary and mobile applications. J Power Sources 2004;127:273–83. doi:10.1016/j.jpowsour.2003.09.024.

[14] Haile SM. Fuel cell materials and components. Acta Mater 2003;51:5981–6000. doi:10.1016/j.actamat.2003.08.004.

[15] Bochentyn B, Karczewski J, Miruszewski T, Krupa A, Gazda M, Jasinski P, et al. Donor-substituted SrTi1 + xO3 - δanodes for SOFC. Solid State Ionics 2012;225:118–23. doi:10.1016/j.ssi.2012.05.015.

[16] Sarin N, Mishra M, Gupta G, Parkin IP, Luthra V. Elucidating iron doping induced n- to p-characteristics of Strontium titanate based ethanol sensors. Curr Appl Phys 2018;18:246–53. doi:10.1016/j.cap.2017.11.007.

[17] Litzelman SJ, Rothschild A, Tuller HL. The electrical properties and stability of SrTi0.65Fe0.35O3−δ thin films for automotive oxygen sensor applications. Sensors Actuators B Chem 2005;108:231–7. doi:10.1016/j.snb.2004.10.040.

[18] Jung W, Tuller HL. Investigation of Cathode Behavior of Model Thin-Film SrTi[sub 1 - x]Fe[sub x]O[sub 3 - delta] (x = 0.35 and 0.5) Mixed Ionic-Electronic Conducting Electrodes. J Electrochem Soc 2008;155:B1194–201. doi:10.1149/1.2976212.

[19] Jung W, Tuller HL. Impedance study of SrTi(1-x)Fe(x)O(3-delta) (x=0.05 to 0.80) mixed ionic-electronic conducting model cathode. Solid State Ionics 2009;180:843–7. doi:10.1016/j.ssi.2009.02.008.

[20] Perry NH, Kim JJ, Tuller HL. Oxygen surface exchange kinetics measurement by simultaneous optical transmission relaxation and impedance spectroscopy: $Sr(Ti,Fe)O_{3-x}$ thin film case study. Sci Technol Adv Mater 2018;19:130–41. doi:10.1080/14686996.2018.1430448.

[21] Rothschild A, Menesklou W, Tuller HL, Ivers-Tiffée E. Electronic structure, defect chemistry, and transport properties of SrTi 1-xFe xO 3-y solid solutions. Chem Mater 2006;18:3651–9. doi:10.1021/cm052803x.

[22] Argirusis C, Jomard F, Wagner SF, Menesklou W, Ivers-Tiffée E. Study of the oxygen incorporation and diffusion in Sr(Ti 0.65Fe0.35)O3 ceramics. Solid State Ionics 2011;192:9–11. doi:10.1016/j.ssi.2010.02.016.

[23] Jung W, Tuller HL. Impedance study of SrTi1-xFexO3-δ (x = 0.05 to 0.80) mixed ionic-electronic conducting model cathode. Solid State Ionics 2009;180:843–7. doi:10.1016/j.ssi.2009.02.008.

[24] Song J-L, Guo X. SrTi0.65Fe0.35O3 nanofibers for oxygen sensing. Solid State Ionics 2015;278:26–31. doi:10.1016/j.ssi.2015.05.009.

[25] Li HY, Yang H, Guo X. Oxygen sensors based on SrTi0.65Fe0.35O3-δthick film with MgO diffusion barrier for automotive emission control. Sensors Actuators, B Chem 2015;213:102–10. doi:10.1016/j.snb.2015.02.079.

[26] Nenning A, Volgger L, Miller E, Mogni L V., Barnett S, Fleig J. The Electrochemical Properties of $Sr(Ti,Fe)O_{3-\delta}$ for Anodes in Solid Oxide Fuel Cells. J Electrochem Soc 2017;164:F364–71. doi:10.1149/2.1271704jes.

[27] Oliveira Silva R, Malzbender J, Schulze-Küppers F, Baumann S, Guillon O. Mechanical properties and lifetime predictions of dense SrTi1-xFexO3-δ(x = 0.25, 0.35, 0.5). J Eur Ceram Soc 2017;37:2629–36. doi:10.1016/j.jeurceramsoc.2017.02.038.

[28] Oliveira Silva R, Malzbender J, Schulze-Küppers F, Baumann S, Krüger M, Guillon O. Microstructure and anisotropic mechanical properties of freeze dried SrTi 0.75 Fe 0.25 O 3-δ for oxygen transport membrane substrates. J Eur Ceram Soc 2018;38:2774–83. doi:10.1016/j.jeurceramsoc.2018.02.014.

[29] Liu Y, Baumann S, Schulze-Küppers F, Mueller DN, Guillon O. Co and Fe co-doping influence on functional properties of SrTiO3for use as oxygen transport membranes. J Eur Ceram Soc 2018;38:5058–66. doi:10.1016/j.jeurceramsoc.2018.07.037.

[30] Baharuddin NA, Muchtar A, Somalu MR. Short review on cobalt-free cathodes for solid oxide fuel cells. Int J Hydrogen Energy 2017;42:9149–55. doi:10.1016/j.ijhydene.2016.04.097.

[31] Liu H, Zhu K, Liu Y, Li W, Cai L, Zhu X, et al. Structure and electrochemical properties of

cobalt-free perovskite cathode materials for intermediate-temperature solid oxide fuel cells. Electrochim Acta 2018;279:224–30. doi:10.1016/j.electacta.2018.05.086.

[32] Rothschild A, Litzelman SJ, Tuller HL, Menesklou W, Schneider T, Ivers-Tiffée E. Temperature-independent resistive oxygen sensors based on SrTi1-xFexO3-δsolid solutions. Sensors Actuators, B Chem 2005;108:223–30. doi:10.1016/j.snb.2004.09.044.

[33] Jung W, Tuller HL. Investigation of Cathode Behavior of Model Thin-Film SrTi[sub 1−x]Fe[sub x]O[sub 3−δ] (x=0.35 and 0.5) Mixed Ionic-Electronic Conducting Electrodes. J Electrochem Soc 2008;155:B1194. doi:10.1149/1.2976212.

[34] Jung W, Tuller HL. Investigation of surface Sr segregation in model thin film solid oxide fuel cell perovskite electrodes. Energy Environ Sci 2012;5:5370–8. doi:10.1039/C1EE02762J.

[35] Jung W, Tuller HL. A New Model Describing Solid Oxide Fuel Cell Cathode Kinetics: Model Thin Film SrTi1- xFexO3- δ Mixed Conducting Oxides–a Case Study. Adv Energy Mater 2011;1:1184–91. doi:10.1002/aenm.201100164.

[36] Yoo C-Y, Bouwmeester HJM. Oxygen surface exchange kinetics of SrTi1−xFexO3−δ mixed conducting oxides. Phys Chem Chem Phys 2012;14:11759. doi:10.1039/c2cp41923h.

[37] Molin S, Lewandowska-Iwaniak W, Kusz B, Gazda M, Jasinski P. Structural and electrical properties of Sr(Ti, Fe)$O_{3-\delta}$ materials for SOFC cathodes. J Electroceramics 2012;28:80–7. doi:10.1007/s10832-012-9683-x.

[38] Jordan N, Assenmacher W, Uhlenbruck S, Haanappel VAC, Buchkremer HP, Stöver D, et al. Ce0.8Gd0.2O2 − δ protecting layers manufactured by physical vapor deposition for IT-SOFC. Solid State Ionics 2008;179:919–23. doi:10.1016/j.ssi.2007.12.008.

[39] Wang F, Nishi M, Brito ME, Kishimoto H, Yamaji K, Yokokawa H, et al. Sr and Zr diffusion in LSCF/10GDC/8YSZ triplets for solid oxide fuel cells (SOFCs). J Power Sources 2014;258:281–9. doi:10.1016/j.jpowsour.2014.02.046.

[40] Szymczewska D, Karczewski J, Chrzan A, Jasinski P. CGO as a barrier layer between LSCF electrodes and YSZ electrolyte fabricated by spray pyrolysis for solid oxide fuel cells. Solid State Ionics 2017;302:113–7. doi:10.1016/j.ssi.2016.11.008.

[41] Li Y, Gemmen R, Liu X. Oxygen reduction and transportation mechanisms in solid oxide fuel cell cathodes. J Power Sources 2010;195:3345–58. doi:10.1016/j.jpowsour.2009.12.062.

[42] Baumann FS, Fleig J, Cristiani G, Stuhlhofer B, Habermeier H-U, Maier J. Quantitative Comparison of Mixed Conducting SOFC Cathode Materials by Means of Thin Film Model Electrodes. J Electrochem Soc 2007;154:B931. doi:10.1149/1.2752974.

[43] Metlenko V, Jung W, Bishop SR, Tuller HL, De Souza RA. Oxygen diffusion and surface exchange in the mixed conducting oxides SrTi $_{1-y}$ Fe $_y$ O $_{3-\delta}$. Phys Chem Chem Phys 2016;18:29495–505. doi:10.1039/C6CP05756J.

[44] Perry NH, Harrington GF, Tuller HL. Electrochemical ionic interfaces. Elsevier Inc.; 2018. doi:10.1016/B978-0-12-811166-6.00004-2.

[45] Degen T, Sadki M, Bron E, König U, Nénert G. The high score suite. Powder Diffr 2014;29:S13–8. doi:10.1017/S0885715614000840.

[46] Momma K, Izumi F. VESTA 3 for three-dimensional visualization of crystal, volumetric and morphology data. J Appl Crystallogr 2011;44:1272–6. doi:10.1107/S0021889811038970.

[47] Koch S, Graves C, Hansen KV. Elchemea Analytical (Open source free software) http://www.elchemea.dk/ n.d.

[48] Ciucci F, Chen C. Analysis of Electrochemical Impedance Spectroscopy Data Using the

Distribution of Relaxation Times: A Bayesian and Hierarchical Bayesian Approach. Electrochim Acta 2015;167:439–54. doi:10.1016/j.electacta.2015.03.123.

[49] Saccoccio M, Wan TH, Chen C, Ciucci F. Optimal regularization in distribution of relaxation times applied to electrochemical impedance spectroscopy: Ridge and Lasso regression methods - A theoretical and experimental Study. Electrochim Acta 2014;147:470–82. doi:10.1016/j.electacta.2014.09.058.

[50] Wan TH, Saccoccio M, Chen C, Ciucci F. Influence of the Discretization Methods on the Distribution of Relaxation Times Deconvolution: Implementing Radial Basis Functions with DRTtools. Electrochim Acta 2015;184:483–99. doi:10.1016/j.electacta.2015.09.097.

[51] Ba¨urer M, Kungl H, Hoffmann MJ. Influence of sr/ti stoichiometry on the densification behavior of strontium titanate. J Am Ceram Soc 2009;92:601–6. doi:10.1111/j.1551-2916.2008.02920.x.

[52] Horikiri F, Iizawa N, Han LQ, Sato K, Yashiro K, Kawada T, et al. Defect equilibrium and electron transport in the bulk of single crystal SrTi1 - xNbxO3(x = 0.01, 0.001, 0.0002). Solid State Ionics 2008;179:2335–44. doi:10.1016/j.ssi.2008.10.001.

[53] Horikiri F, Han L, Iizawa N, Sato K, Yashiro K, Kawada T, et al. Electrical Properties of Nb-Doped SrTiO[sub 3] Ceramics with Excess TiO[sub 2] for SOFC Anodes and Interconnects. J Electrochem Soc 2008;155:B16. doi:10.1149/1.2799733.

[54] Acharya SK, Nallagatla RV, Togibasa O, Lee BW, Liu C, Jung CU, et al. Epitaxial Brownmillerite Oxide Thin Films for Reliable Switching Memory. ACS Appl Mater Interfaces 2016;8:7902–11. doi:10.1021/acsami.6b00647.

[55] Lytle FW. X-ray diffractometry of low-temperature phase transformations in strontium titanate. J Appl Phys 1964;35:2212–5. doi:10.1063/1.1702820.

[56] Kharton V V., Kovalevsky A V., Viskup AP, Jurado JR, Figueiredo FM, Naumovich EN, et al. Transport properties and thermal expansion of Sr0.97Ti1-xFexO3-δ(x = 0.2-0.8). J Solid State Chem 2001;156:437–44. doi:10.1006/jssc.2000.9019.

[57] Kharton V V., Kovalevsky A V., Tsipis E V., Viskup AP, Naumovich EN, Jurado JR, et al. Mixed conductivity and stability of A-site-deficient Sr(Fe,Ti)O 3-δ perovskites. J Solid State Electrochem 2003;7:30–6. doi:10.1007/s10008-002-0286-3.

[58] Jurado JR, Figueiredo FM, Gharbage B, Frade JR. Electrochemical permeability of Sr-0.7(Ti,Fe)O3-delta materials. Solid State Ionics 1999;118:89–97. doi:Doi: 10.1016/s0167-2738(98)00471-8.

[59] Menesklou W, Schreiner H-J, Härdtl KH, Ivers-Tiffée E. High temperature oxygen sensors based on doped SrTiO3. Sensors Actuators B Chem 1999;59:184–9. doi:http://dx.doi.org/10.1016/S0925-4005(99)00218-X.

[60] Moos R, Menesklou W, Schreiner HJ, Härdtl KH. Materials for temperature independent resistive oxygen sensors for combustion exhaust gas control. Sensors Actuators, B Chem 2000;67:178–83. doi:10.1016/S0925-4005(00)00421-4.

[61] Steinsvik S, Bugge R, Gjønnes J, Taftø J, Norby T. The defect structure of SrTi 1−x Fe x O 3−y (x = 0–0.8) investigated by electrical doncutivity measurements and electron energy loss spectroscopy (EELS). J Phys Chem Solids 1997;58:969–76. doi:10.1016/S0022-3697(96)00200-4.

[62] Yu X, Long W, Jin F, He T. Cobalt-free perovskite cathode materials SrFe1-xTixO3-δand performance optimization for intermediate-temperature solid oxide fuel cells. Electrochim Acta 2014;123:426–34. doi:10.1016/j.electacta.2014.01.020.

[63] Mogensen M, Sammes NM, Tompsett GA. Physical, chemical and electrochemical properties of pure and doped ceria. Solid State Ionics 2000;129:63–94. doi:10.1016/S0167-2738(99)00318-5.

[64] Tsipis E V., Kharton V V. Electrode materials and reaction mechanisms in solid oxide fuel cells: a brief review. J Solid State Electrochem 2007;12:1039–60. doi:10.1007/s10008-007-0468-0.

[65] Chen Y, Zhou W, Ding D, Liu M, Ciucci F, Tade M, et al. Advances in Cathode Materials for Solid Oxide Fuel Cells: Complex Oxides without Alkaline Earth Metal Elements. Adv Energy Mater 2015;5:n/a-n/a. doi:10.1002/aenm.201500537.

[66] Chrzan A, Gazda M, Szymczewska D, Jasinski P. Interaction of SrTi0.65Fe0.35O3-δ with LaNi0.6Fe0.4O3-δ, La0.6Sr0.4Co0.2Fe0.8O3-δ and Ce0.8Gd0.2O2-δ. Procedia Eng 2014;98:101–4. doi:10.1016/j.proeng.2014.12.494.

[67] Takeda Y. Cathodic Polarization Phenomena of Perovskite Oxide Electrodes with Stabilized Zirconia. J Electrochem Soc 1987;134:2656. doi:10.1149/1.2100267.

[68] Esquirol A, Brandon NP, Kilner JA, Mogensen M. Electrochemical Characterization of La[sub 0.6]Sr[sub 0.4]Co[sub 0.2]Fe[sub 0.8]O[sub 3] Cathodes for Intermediate-Temperature SOFCs. J Electrochem Soc 2004;151:A1847. doi:10.1149/1.1799391.

[69] Boukamp BA, Rolle A. Use of a distribution function of relaxation times (DFRT) in impedance analysis of SOFC electrodes. Solid State Ionics 2018;314:103–11. doi:10.1016/j.ssi.2017.11.021.

[70] Boukamp B a., Hildenbrand N, Nammensma P, Blank DH a. The impedance of thin dense oxide cathodes. Solid State Ionics 2011;192:404–8. doi:10.1016/j.ssi.2010.05.037.

[71] Hildenbrand N. Improving the electrolyte - cathode assembly for mt-SOFC. 2011.

[72] Adler SB. Factors governing oxygen reduction in solid oxide fuel cell cathodes. Chem Rev 2004;104:4791–843. doi:10.1021/cr020724o.

[73] Lu Y, Kreller C, Adler SB. Measurement and Modeling of the Impedance Characteristics of Porous La[sub 1−x]Sr[sub x]CoO[sub 3−δ] Electrodes. J Electrochem Soc 2009;156:B513. doi:10.1149/1.3079337.

[74] Dailly J, Fourcade S, Largeteau A, Mauvy F, Grenier JC, Marrony M. Perovskite and A2MO4-type oxides as new cathode materials for protonic solid oxide fuel cells. Electrochim Acta 2010;55:5847–53. doi:10.1016/j.electacta.2010.05.034.

[75] Nenning A, Opitz AK, Huber TM, Fleig J. A novel approach for analyzing electrochemical properties of mixed conducting solid oxide fuel cell anode materials by impedance spectroscopy. Phys Chem Chem Phys 2014;16:22321–36. doi:10.1039/c4cp02467b.

[76] dos Santos-Gómez L, Porras-Vázquez JM, Losilla ER, Marrero-López D. Improving the efficiency of layered perovskite cathodes by microstructural optimization. J Mater Chem A 2017:7896–904. doi:10.1039/C6TA10946B.